HAL
open science

ZnO under Pressure: From Nanoparticles to Single Crystals

Andrei Baranov, Petr Sokolov, Vladimir Solozhenko

To cite this version:

Andrei Baranov, Petr Sokolov, Vladimir Solozhenko. ZnO under Pressure: From Nanoparticles to Single Crystals. Crystals, 2022, 12 (5), pp.744. 10.3390/cryst12050744 . hal-03676470

HAL Id: hal-03676470

https://hal.science/hal-03676470

Submitted on 24 May 2022

HAL is a multi-disciplinary open access archive for the deposit and dissemination of scientific research documents, whether they are published or not. The documents may come from teaching and research institutions in France or abroad, or from public or private research centers.

L'archive ouverte pluridisciplinaire **HAL**, est destinée au dépôt et à la diffusion de documents scientifiques de niveau recherche, publiés ou non, émanant des établissements d'enseignement et de recherche français ou étrangers, des laboratoires publics ou privés.

Review

ZnO under Pressure: From Nanoparticles to Single Crystals

Andrei N. Baranov [1], Petr S. Sokolov [2] and Vladimir L. Solozhenko [3,*]

[1] Lomonosov Moscow State University, 119991 Moscow, Russia; anb@inorg.chem.msu.ru
[2] National Research Center "Kurchatov Institute"—IREA, 123098 Moscow, Russia; sokolov-petr@yandex.ru
[3] LSPM–CNRS, Université Sorbonne Paris Nord, 93430 Villetaneuse, France
* Correspondence: vladimir.solozhenko@univ-paris13.fr

Abstract: In the present review, new approaches for the stabilization of metastable phases of zinc oxide and the growth of ZnO single crystals under high pressures and high temperatures are considered. The problems of the stabilization of the cubic modification of ZnO as well as solid solutions on its basis are discussed. A thermodynamic approach to the description of zinc oxide melting at high pressures is described which opens up new possibilities for the growth of both undoped and doped (for example, with elements of group V) single crystals of zinc oxide. The possibilities of using high pressure to vary phase and elemental composition in order to create ZnO-based materials are demonstrated.

Keywords: zinc oxide; high pressure; phase transitions; solid solutions; metastable phases; semiconductor properties; single crystals

1. Introduction

Zinc oxide is a promising semiconductor material that has high potential for a wide variety of applications, such as light-emitting diodes, sensors, solar cells, photocatalysts, etc. [1–4]. Its semiconductor properties are usually controlled by doping. In this case, the main goal is to control the transport properties. At the same time, the introduction of transition metal cations into the zinc oxide matrix makes it possible to control the charge carrier spin as well, which leads to a combination of semiconducting and magnetic properties [5]. At ambient pressure ZnO crystallizes in a hexagonal wurtzite structure (w-ZnO, $P6_3mc$). The high-pressure phase of zinc oxide with a cubic rock-salt structure (rs-ZnO, Fm-$3m$) has also been known for quite a long time [6]. There are a few publications on the possible existence of other crystal structures of ZnO, but all these phases have no thermodynamic stability regions and are not considered in this review. For the practical application of zinc oxide as a semiconductor material it is necessary to be able to control the type and concentration of carriers and, if possible, the band gap (Eg). The first problem is usually solved by doping (i.e., by introducing either a donor or an acceptor impurity at the desired concentration), and the second by forming solid solutions. Whereas a small quantity of introduced impurity is sufficient to solve the first problem, the second one often requires a significant number of foreign element(s). However, wurtzite ZnO imposes rather strong restrictions on the practically achievable amount of inserted impurity which usually does not exceed several atomic percent (for instance, the solubility limit of Ni^{2+} in w-ZnO is 0.9 mol% at 1073 K) [7]. The tetrahedral oxygen environment in the wurtzite structure does not allow the dopant concentration to be varied over a wide range and therefore, the semiconducting properties of zinc oxide cannot be effectively controlled. The most successful examples realized in practice are either the introduction of three-charged cations (such as aluminum, iron, indium, gallium) at zinc position, or the substitution of oxygen with fluorine to create donor centers [8]. In this way, transparent conductive coatings are obtained as an alternative to high-cost indium tin oxide substrates.

Numerous attempts were made to introduce acceptor centers into ZnO. Elements of the first and fifth groups, as well as some others were used for this purpose [4]. Despite the huge number of publications on the subject, none of the proposed approaches has reached practical implementation.

The control of the band gap is not the best situation either. This problem is especially relevant for photocatalytic applications [9,10] where it is necessary to shift the band gap into the visible light region. For w-ZnO, there are only minor successes in controlling Eg over a rather narrow range.

In the case of rs-ZnO, the above-mentioned restrictions are absent. The octahedral oxygen environment removes the crystallochemical limitations for the introduction of a variety of cations. Thus, it is possible to tune the properties in the wide range of dopant concentrations while remaining in the solid solution stability field. Examples of materials that are interesting from the point of view of semiconducting properties are ZnO solid solutions with magnesium oxide [11,12] and nickel oxide [13,14]. Research is developing in two directions: epitaxial stabilization of rs-ZnO in thin films on oriented substrates [11–14] and high-pressure phase transformation of the wurtzite phase to the cubic one [15,16].

Although the first report on the observation of zinc oxide phase transformation into the cubic modification was made many years ago [6], this work is still relevant. The main problem that remains to be overcome by researchers (except the authors of the work [17]) is a complete recovery of cubic ZnO at ambient pressure.

In the present paper we will consider the high-pressure synthesis and properties of cubic zinc oxide and related materials (see Figure 1). In particular:

1. Synthesis of cubic ZnO solid solutions with MeO (where Me = Mg^{2+}, Ni^{2+}, Co^{2+}, Fe^{2+}, Mn^{2+}) and with $LiMeO_2$ (where Me = Sc^{3+}, Ti^{3+}, Fe^{3+}, In^{3+}), and their thermal stability at ambient pressure.
2. Synthesis of rs-ZnO using the nanocrystalline state of the initial wurtzite phase, including synthesis in the sodium chloride and magnesium oxide matrixes.
3. Growth of zinc oxide single crystals from melts at high pressures and high temperatures (HP and HT).

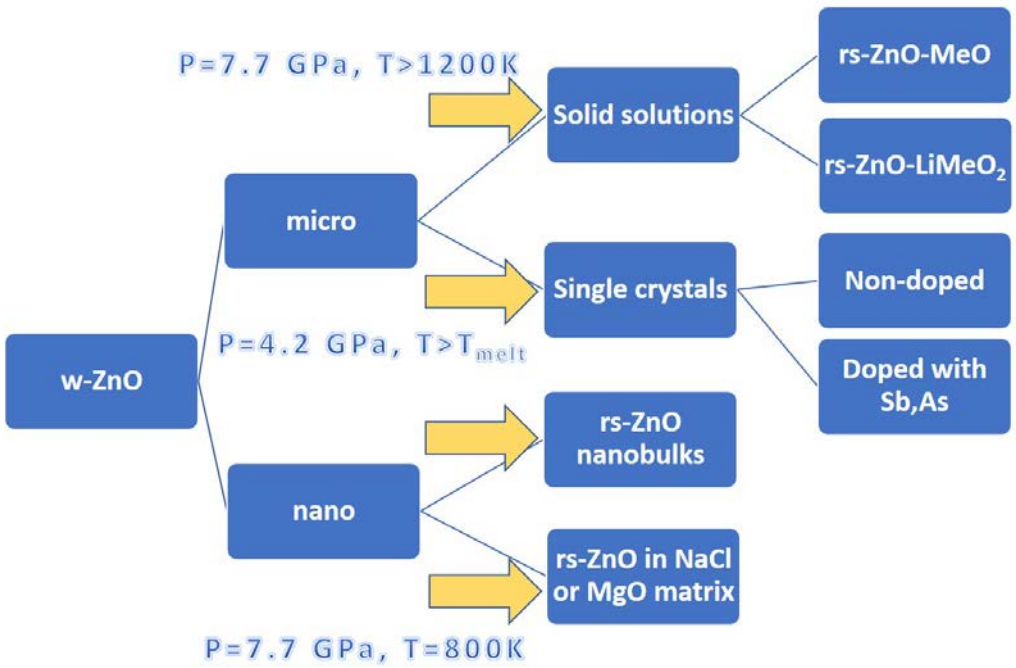

Figure 1. The scheme of high-pressure production of new phases, morphological forms and solid solutions based on zinc oxide.

We will also consider the fundamental thermodynamic parameters characterizing the phase transformations of ZnO at high and ambient pressures.

2. Results and Discussion

2.1. Wurtzite ZnO

The most important features of w-ZnO include high exciton binding energy, radiation resistance, nontoxicity, a low thermal expansion coefficient, and high chemical and thermal stability. The elemental cell of w-ZnO contains two formula units. Oxygen atoms form the hexagonal close-packed lattice while zinc atoms are located in the centers of slightly distorted tetrahedrons, i.e., half of the tetrahedral cavities formed by oxygen atoms are filled (Figure 2, top left). The structure is characterized by the absence of a symmetry center so the crystals have a polar axis parallel to the [0001] direction and exhibit pyro- and piezoelectric properties. At ambient pressure, ZnO retains the wurtzite structure up to the point of melting (triple point 2248 K, 0.106 MPa) [18].

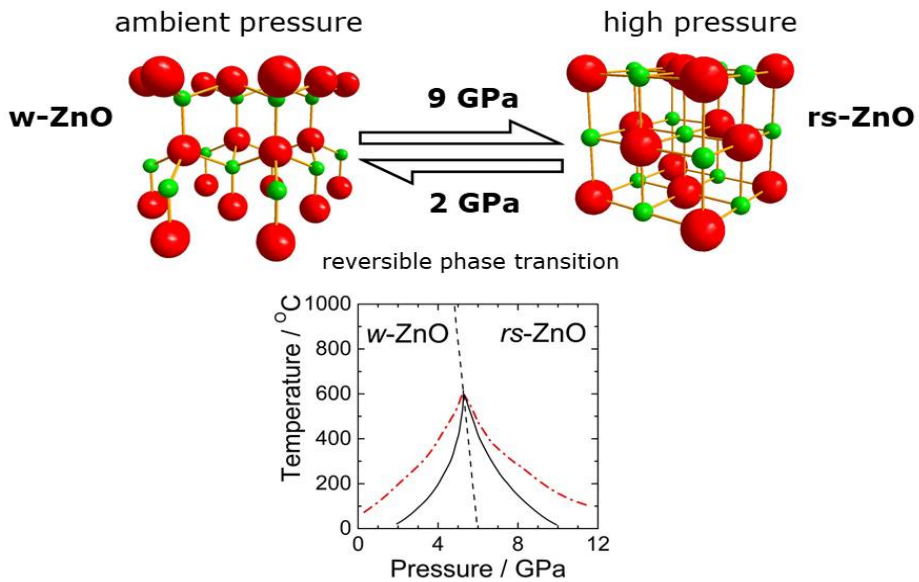

Figure 2. Direct and inverse phase transitions in ZnO [19] (black lines). Hypothetical hysteresis for nanocrystalline ZnO is shown by red lines.

Zinc oxide is an alternative material to GaN in the field of UV optoelectronics. It is less expensive, more available, and considered to be an efficient light-emitting material. Impurity doped w-ZnO can be used both as a conductive oxide transparent to visible light [8,20] and as a potential candidate for semiconductor spintronics. Among binary semiconductors it has a record high exciton binding energy (~60 meV in comparison with 26 meV for GaN, 22 meV for ZnSe and 4.2 meV for GaAs [2,4]) which provides the presence of a UV luminescence band caused by direct exciton recombination up to 500 K. The luminescence spectra of w-ZnO usually have two characteristic emission bands—a narrow band in the UV region ($\lambda \approx 380$ nm, $\Delta\lambda \approx 15$ nm) and a broad band in the visible region ($\lambda \approx 520$ nm, $\Delta\lambda \approx 100$ nm) [20].

Doping zinc oxide with other metal cations allows the modification of its functional properties, thus achieving a change in the photoluminescence character, electrical properties, and the appearance of weak ferromagnetism [21,22]. Doping with cadmium oxide

or magnesium oxide modifies the band gap of w-ZnO [23]. Thus, using nonequilibrium methods to produce materials, particularly films, one can achieve a significant increase in the concentration of the second component [23].

2.2. w-ZnO → rs-ZnO Phase Transition

The transition of w-ZnO to rs-ZnO at room temperature occurs at pressures of about 9.5 GPa [6,19,24]. At the subsequent pressure decrease, the cubic structure is preserved down to 2 GPa [19,24]. Thus, there is a significant hysteresis between the direct (w-ZnO → rs-ZnO) and inverse (rs-ZnO → w-ZnO) transitions at room temperature. As the temperature increases, the width of the hysteresis loop decreases and above 1200 K the direct and inverse transition branches converge at a pressure of ~5 GPa [19,24]. This can be considered as the equilibrium pressure of this phase transition at high temperatures (Figure 2).

The slope (dP/dT) of the rs-ZnO → w-ZnO transition line was reported to be close to zero (without specifying a sign) [24]. Other works give values of −0.0012 GPa/K [19]; 0.00425 GPa/K [6]; and dP/dT < 0 (but not significantly different) [25]. Note that according to the Clapeyron-Clausius relation, the sign of dP/dT (dP/dT = ΔH/(TΔV)) is directly related to the sign of the enthalpy of w-ZnO → rs-ZnO transition. In the theoretical work of [26], the position of the w-ZnO ⇄ rs-ZnO equilibrium line in the P-T phase diagram was claimed to be different from the experimental data [19,24]. Thus, one can see that the results presented in the literature are rather contradictory and until the cubic zinc oxide phase was recovered at ambient pressure [17] even the sign of the w-ZnO → rs-ZnO transformation enthalpy was not known.

The w-ZnO → rs-ZnO phase transition under pressure has been in situ studied in several experimental works. A variety of methods and initial states of zinc oxide (single crystals, polycrystalline bulks and powders, and films) were used. Thus, phase transition in a monocrystalline zinc oxide was studied by single crystal X-ray diffraction [27] and ultrasonic wave velocity measurements [28]. Phase transition in thin films was studied by optical absorption and photoluminescence measurements [29,30]. The possible band structure of rs-ZnO is discussed in [29,30]. According to the estimations made, rs-ZnO is an indirect-gap semiconductor with a bandgap of 2.45 ± 0.15 eV [29] (or 2.7 ± 0.2 eV [30]).

The phase transition in polycrystalline samples was studied by energy-dispersive synchrotron X-ray diffraction [24,31], electrical resistivity measurements [31,32], X-ray-absorption spectroscopy [33], ^{67}Zn-Mössbauer spectroscopy [34], Raman spectroscopy [35,36], and optical second harmonic generation measurements [37]. Based on all data available in the literature, we can confidently conclude that the w-ZnO → rs-ZnO transition is a classical first-order transition without formation of intermediate phase(s).

Zinc is known to complete the series of 3D transition metals such as Mn, Co, Fe, Ni, and Cu. All monoxides of these metals are semiconductors with p-type conductivity. It cannot be excluded that rs-ZnO and solid solutions based on it will also have p-type conductivity. This could be very useful for forming a homogeneous p-n junction in ZnO-based semiconductor structures. Previously, in situ measurements of rs-ZnO conductivity at room temperature and pressures up to 18 GPa [31] and 35 GPa [32] were reported. It was shown that rs-ZnO has a semiconductor (nonmetallic) type of conductivity, in contrast to its closest analogue rs-ZnS for which metallic type conductivity was found [38].

The optical properties of rs-ZnO thin films were studied in [29,30]. The authors found that cubic zinc oxide is an indirect-gap semiconductor with Eg = 2.7 ± 0.2 eV (at 11 GPa, 300 K). The band structure of rs-ZnO was calculated ab initio by DFT using LDA pseudopotential [30]. It was shown that the conduction band minimum located at the Γ point is about 1.1 eV above the valence band maxima located at the *L* point. The direct transitions at X and L points were predicted at 5.6 and 7.6 eV, respectively. The lowest direct transition at the Γ point was assigned at ~4.5 eV (at 11 GPa).

2.3. Stabilization of rs-ZnO in the Form of Solid Solutions

The kinetic stabilization of metastable rs-ZnO at ambient pressure can be achieved by quenching ZnO-based solid solutions with a relatively high (up to 80 mol%) ZnO content from HP and HT [15,16,39–44]. Two types of rs-ZnO cation-substitution solid solutions have been considered, i.e., $Zn^{2+} \leftrightarrow Me^{2+}$ (type I) and $2\,Zn^{2+} \leftrightarrow Li^{+} + Me^{3+}$ (type II).

The formation of type I solid solutions under HP and HT has been demonstrated using in-situ energy-dispersive synchrotron X-ray diffraction for the MgO-ZnO [16], FeO-ZnO [42], MnO-ZnO [41,43], CoO-ZnO [40] and NiO-ZnO systems [40], as well as by the quenching (from 7.7 GPa and 1450–1550 K) technique [15,39]. Generally, under a pressure of about 5 GPa at temperatures below ~750 K only reflections of initial oxides (w-ZnO and rs-MeO) are seen in the diffraction patterns. Upon heating, the chemical interaction between oxides leads to w-ZnO dissolution in rs-MeO and the formation of a cubic solid solution. The onset temperature of this interaction (T_s) weakly depends on the reaction mixture stoichiometry ($0.3 \le x \le 0.85$), see Figure 3. As usual, the formed rs-$Me_{1-x}Zn_xO$ solid solution coexists with w-ZnO and rs-MeO in a wide temperature range (up to 1100–1300 K). During further heating, the reflexes of initial oxide w-ZnO and rs-MeO disappear completely and only lines of rs-$Me_{1-x}Zn_xO$ solid solution are observed. The completion temperature of the chemical interaction (T_d) more strongly depends on the initial stoichiometry and increases markedly with the increase in ZnO content [40,42,43].

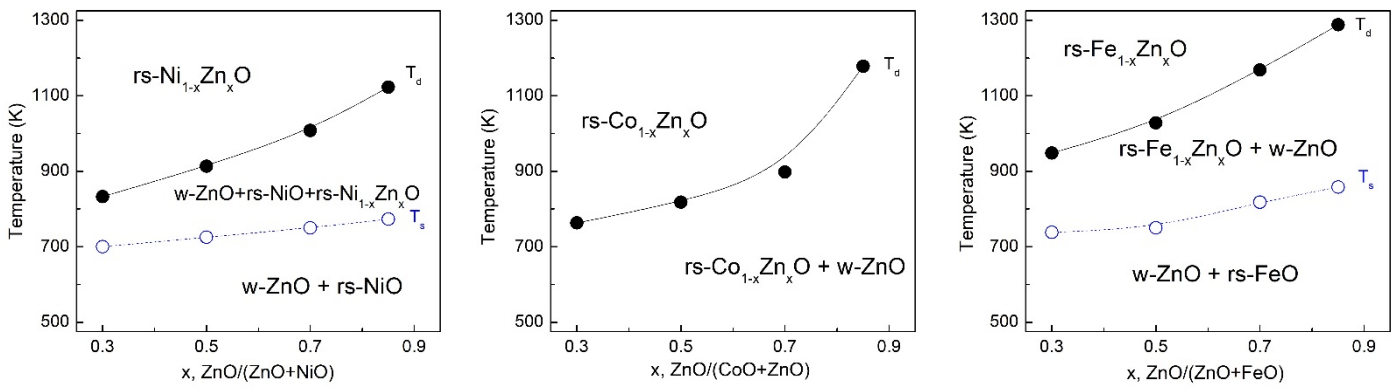

(**a**) (**b**) (**c**)

Figure 3. (**a**) The onset (T_s) and completion (T_d) temperatures of chemical interaction in the NiO-ZnO (**a**), CoO-ZnO (**b**) and FeO-ZnO (**c**) systems versus stoichiometry at 4.9 GPa [40,42,43]. Open circles show the temperatures when lines of cubic solid solution appear in the diffraction patterns while solid circles correspond to the temperatures when lines of wurtzite ZnO disappear completely.

It is easy to see that under high pressure the completion temperature of the chemical interaction between w-ZnO and rs-MeO depends on the nature of the Me^{2+} cation. The interaction between CoO and w-ZnO is completed at a lower temperature than for other metal monoxides, probably because they both share the same ionic radii (0.74 Å) of Co^{2+} and Zn^{2+} [45]. The interaction of w-ZnO with NiO and FeO is completed at higher temperatures. Finally, the interaction between MnO and w-ZnO [43] requires even higher temperatures, apparently due to the largest difference between the ionic radii of Mn^{2+} (0.83 Å) and Zn^{2+}. The diffusion of Me^{2+} cations with sizes different from that of Zn^{2+} is obviously somewhat retarded.

Extrapolation of T_d temperature to x = 1 (pure ZnO) for all investigated systems [40,42,43] gives 1400(50) K which perfectly agrees with the data from work [19]. Thus, 1400 K value can be considered as the equilibrium temperature of the w-ZnO → rs-ZnO phase transition at a pressure of about 4.9 GPa.

Thus, a series of ZnO-based solid solutions with a rock-salt structure have been synthesized at HP and HT in large-volume high-pressure apparatuses and then quenched down to ambient conditions [39–44]. The results for the type I solid solutions are shown in Figure 4 and Table 1.

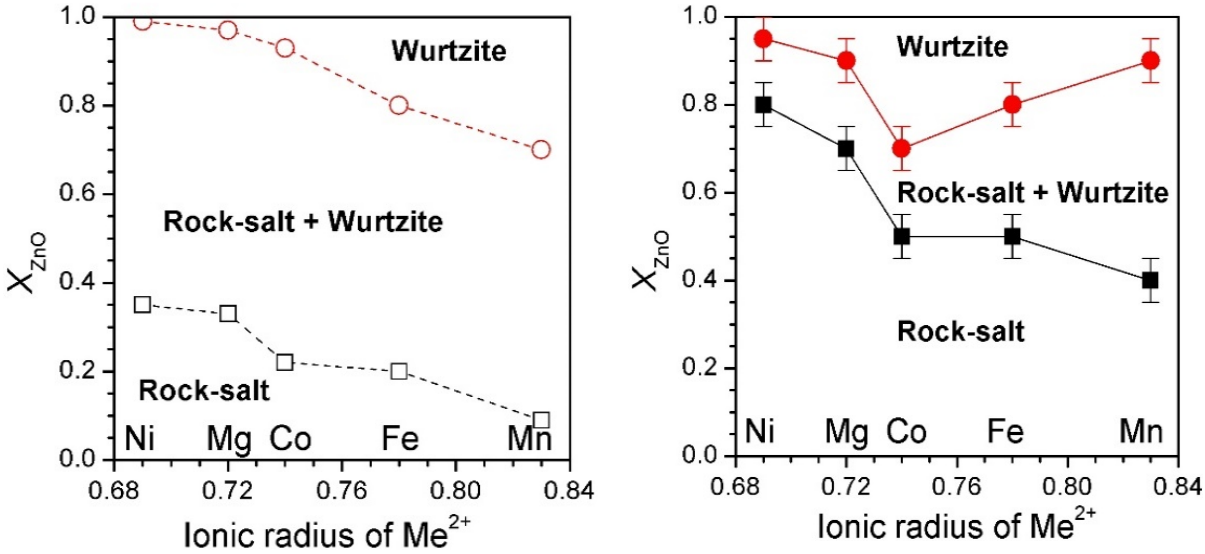

(**a**) (**b**)

Figure 4. Phase composition in the ZnO-MeO systems as a function of the Me^{2+} ionic radius: (**a**) at ambient pressure and 1100 K [7,46]; and (**b**) after quenching from 7.7 GPa and 1500 K [15,39,40].

Table 1. Phase composition of type I solid solutions with different ZnO/(MeO+ZnO) ratio after quenching from 7.7 GPa and 1450-1650 K [15,39,40].

ZnO Mole Fraction, x	NiO-ZnO	MgO-ZnO	CoO-ZnO	FeO-ZnO	MnO-ZnO
0.95	w	w	w	w	w
0.90	w + rs	w	w	w	w
0.80	rs	w + rs	w	w	w + rs
0.70	rs	rs	w	w	w + rs
0.60	rs	rs	w + rs	rs + w	rs + w
0.50	rs	rs	rs	rs	rs + w
0.40	rs	rs	rs	rs	rs
0.30	rs	rs	rs	rs	rs
0.20	rs	rs	rs	rs	rs
0.10	rs	rs	rs	rs	rs
0.00	rs	rs	rs	rs	rs

Note: Cation radii (in Å): Ni^{2+}—0.69, Mg^{2+}—0.72, Co^{2+}—0.74, Fe^{2+}—0.78, Mn^{2+}—0.83 [45].
The colors visualize the concentration regions of formation of solid solutions with different structures.

One can see that the nature of the cation has a significant effect on the formation of cubic solid solutions. The key parameters are the charge and size of the cation. For type I solid solutions, the cation should be stable in the oxidation state +2 and the size should be close to the size of Zn^{2+} (0.74 Å for coordination number 6 [45]). Only five chemical elements satisfy these conditions, namely nickel, magnesium, iron, cobalt and manganese. For all these elements, the concentration range of the $Me_{1-x}Zn_xO$ cubic solid solutions has been extended under pressure. For example, at ambient pressure and 1100 K ZnO solubility in nickel (II) oxide is only 0.35, while $Ni_{0.2}Zn_{0.8}O$ solid solution (x = 0.8) still has a rock-salt-type structure (see Figure 4a, [7]). Thus, HP and HT synthesis allowed the expansion of the stability range of $Ni_{1-x}Zn_xO$ cubic solid solutions. A similar situation is observed for other systems as well. For the FeO-ZnO and CoO-ZnO systems the ZnO

content in the cubic solid solutions synthesized at HP&HT reaches 0.5. This is noticeably higher than that at ambient pressure. For the MnO-ZnO system the highest ZnO content of the cubic solid solutions after HP and HT treatment is 0.4 ($Mn_{0.6}Zn_{0.4}O$) [39,40] (or 0.5 according to another group [41]). At ambient pressure and 1100 K the ZnO solubility limit in MnO is below 0.1 (see Figure 4a). The feature of the MnO-ZnO solid solutions is that the range of co-existence of the two phases (cubic and wurtzite) after quenching from HP and HT remains wide enough, i.e., $0.5 \leq x \leq 0.9$ (Figure 4b). For x = 0.7–0.8 the dominant phase is wurtzite, and for x = 0.5–0.6 the dominant phase is cubic.

Is it possible to expand the range even further towards cubic ZnO? The increase in synthesis parameters does not change the situation, so another approach has been used [47]—namely, the HP and HT synthesis was performed in the presence of sodium chloride. As a result, $Co_{1-x}Zn_xO$ cubic solid solutions in NaCl matrix have been stabilized up to x = 0.8, whereas without the salt matrix the maximum x-value is only 0.5 (see Table 1). It is worth noting that the solid solutions synthesized in this way may be washed out from the salt matrix by cold water and retain their cubic structure [40].

The thermal stability of rock-salt ZnO-based solid solutions at ambient pressure has been studied by high-temperature synchrotron X-ray diffraction [40]. It was found that these solid solutions are kinetically stable up to 670–1000 K depending on the composition (x) and nature of Me^{2+} cation. For instance, the cubic structure of $Ni_{0.2}Zn_{0.8}O$ is stable up to 970 K. The cubic phase of $Co_{0.3}Zn_{0.7}O$ remains stable until 673 K and $Co_{0.4}Zn_{0.6}O$ is stable up to 773 K. According to [41], the cubic phase of $Zn_{0.3}Mn_{0.7}O$ remains stable up to 773 K and this is in good agreement with our unpublished data. The decomposition products are mixtures of two solid solutions, one with cubic structures and another with wurtzite structures. At room temperature, all the synthesized metastable cubic solid solutions show no tendency to reverse transition into a wurtzite structure over several years.

The possibility of substitution not only in the cation, but also in the anion sublattice was also studied. There are only two potential candidates for such substitution, i.e., F^- (1.33 Å) and S^{2-} (1.84 Å). Only these anions have the ionic radii close to the ionic radius of O^{2-} (1.40 Å) [45]. A special series of experiments were performed at 7.7 GPa and 1500 K in order to synthesize the solid solutions in the ZnO-LiF (1:1 molar ratio) and ZnO-ZnS (19:1 molar ratio) systems. In both cases, no chemical interaction was observed. According to X-ray diffraction data, after quenching down to ambient conditions the samples were mixtures of w-ZnO, rs-ZnO and rs-LiF in the first case and w-ZnO and zb-ZnS in the second case. Thus, it has been experimentally shown that attempts to stabilize cubic ZnO via synthesis of solid solutions by substitution in the anion sublattice were unsuccessful.

The main feature of the ZnO-$LiMeO_2$ systems is the fact that at ambient pressure zinc oxide does not form any solid solution with $LiMeO_2$. However, a HP and HT-synthesis of extensive type II solid solutions of have been reported for $LiTiO_2$ [40,44], $LiInO_2$ [40,48], $LiScO_2$ [40,48] and $LiFeO_2$ [40,44]. For the mentioned ternary systems, the kinetic stabilization of metastable rs-ZnO can probably be explained by the close ionic radii of Zn^{2+} (0.74 Å) and Li^+ (0.76 Å [45]), and the smaller ionic radii of transition metals. A smaller radius cation "compresses" the crystal lattice (the known effect of "chemical pressure" [49]) which leads to the stabilization of the cubic structure of a forming solid solution. Moreover, the strong ionicity of the Li–O bond (lithium electronegativity is the lowest among all considered metals) is a favorable factor. Further, it should be noted that in an oxygenated environment Li+ cation has an energy preference for occupying the octahedral position in comparison with the tetrahedral position [50]. The results for the type II solid solutions are presented in Table 2.

Table 2. Phase composition of the xZnO–(1-x)$LiMeO_2$ type II solid solutions quenched from 7.7 GPa and 1250–1450 K [40,44,48].

Solute	Cation radius (Å) [45]	Range and structure of solid solutions
$LiTiO_2$	Ti^{3+} (0.67)	x > 0.8 (w + rs); x ≤ 0.8 (rs)
$LiFeO_2$	Fe^{3+} (0.74)	x > 0.8 (w + rs); x ≤ 0.8 (rs)
$LiScO_2$	Sc^{3+} (0.74)	x > 0.8 (w + rs); 0.5 ≤ x ≤ 0.8 (rs)
$LiInO_2$	In^{3+} (0.80)	x > 0.8 (w + rs); 0.5 ≤ x ≤ 0.8 (rs)

For all ternary systems, the onset of the thermal decomposition of solid solutions depends on ZnO concentration. For example, at x = 0.6 rock-salt $(LiFeO_2)_{1-x}(ZnO)_x$ is kinetically stable at an ambient pressure up to 770 K, but at x = 0.8 it starts to decompose already at 673 K [44]. The nature of Me^{3+} cation has a strong impact on the thermal stability of the rock-salt phase as well. Rock-salt $(LiScO_2)_{0.3}(ZnO)_{0.7}$ is stable up to 820 K whereas $(LiFeO_2)_{0.3}(ZnO)_{0.7}$ is stable up to 720 K only [40,44,48].

The same limiting value of x ≈ 0.8 for both binary (ZnO-NiO, ZnO-CoO) and ternary (ZnO-$LiMeO_2$) oxides systems suggests that this value is most likely not a random one. On average, 0.8 (i.e., less than 1) Me^{2+} or $(LiMe^{3+})_{0.5}$ cation is presented per the unit cell, containing four formula units. For the limiting compositions, about 10 of 12 positions in the second coordination sphere (Zn-Me) are occupied by zinc atoms. The close solubility limits for cubic solid solutions in ZnO-MgO (x ≈ 0.85 [11] and x ≈ 0.82 [12]) and ZnO-NiO (x ≈ 0.73) [13,14] thin films have recently been reported.

Some structural [51–55], optical [56–62] and magnetic [40,52] properties of recovered cubic ZnO-based solid solutions were studied under ambient pressure. The fine crystalline structure of cubic $Ni_{1-x}Zn_xO$ [51,52] and $Mg_{1-x}Zn_xO$ [53] solid solutions has been examined in a wide concertation range by X-ray powder diffraction. It has been found that the diffraction patterns of these compounds contain a system of superlattice diffuse lines, the number and intensity of which depend on the composition [51,52]. It was found that an integrated intensity ratio between the *111* and *002* reflections correlated with zinc fraction in polycrystalline $Mg_{1-x}Zn_xO$ solid solutions [53]. The local structure of cubic $Ni_{1-x}Zn_xO$ solid solutions has been studied by EXAFS spectroscopy and the existence of bounded chaos in the system of oxide solid solutions was discovered [54,55]. It is shown for ZnO-rich solid solution that the ideal rock-salt lattice is distorted and long-range order exists only on the average (Vegard's law) [54,55].

Thus, a series of metastable ZnO-based solid solutions with a rock-salt structure have been synthesized by quenching from 7.7 GPa and 1350–1550 K. At ambient pressure these solutions can be retained in the wide concentration range (up to 0.8 ZnO molar fraction) but decomposes on heating above 670–1000 K (depending on the composition). It was shown that the cation radius (r) in the rs-ZnO lattice can vary over a wide range, namely, from 0.67 Å (Ti^{3+}) to 0.83 Å (Mn^{2+}), and cation charge (n) can take values of 2 and 3. This wide variation in size and charge for substituted cations is not generally characteristic of oxide systems (such as MgO or CaO), and thus, may open up new prospects for fundamental and applied science. Some ZnO-based solid solutions with a rock-salt structure synthesized under HP and HT may be of interest as promising Li-containing materials [13,14,63–69] or materials with high dielectric characteristics [66–69]. The described approach to stabilize rock-salt ZnO can also be used in other systems that include high-pressure phases that are difficult to quench.

2.4. Synthesis of Single-Phase rs-ZnO Nanobulks

As for pure zinc oxide, the direct transition of nanocrystalline w-ZnO is observed at a much higher pressure (>9 GPa) than that of microcrystalline zinc oxide [31, 70–73]. w-ZnO powders with a particle size of ~12 nm undergo the transition at P ≈ 15 GPa [31]. This fact was explained by significant contribution of surface energy which should be considered for highly dispersed powders [31, 70–72]. After recovery at ambient pressure,

the samples usually represented a mixture of w-ZnO and rs-ZnO [71,73]. Thus, several experimental works have shown that the nanocrystalline state of initial w-ZnO shifts the boundary of the direct w-ZnO → rs-ZnO transition to the high-pressure region. This leads to the expectation of a decrease in the pressure of the inverse rs-ZnO → w-ZnO transition down to the ambient, i.e., kinetic stabilization of rs-ZnO under normal conditions (see the red line in Figure 2).

To test this hypothesis, a series of experiments using salt (w-ZnO/NaCl) [47] and oxide (ZnO/MgO) [74] matrices and monodisperse nanocrystalline w-ZnO powders [17] as starting materials were performed at 7.7 GPa and 800 K. In all cases, rs-ZnO without w-ZnO impurity was recovered. It was established that single-phase rock-salt zinc oxide can be quenched if two conditions are met: (i) w-ZnO nanopowder should be synthesized by "chemically route" and (ii) the crystallite size in initial w-ZnO powder should be less than 45 nm [17] (see Figure 5). If initial w-ZnO powder contains a fraction with a larger particle size, the result is likely to be a mixture of two phases, w-ZnO and rs-ZnO.

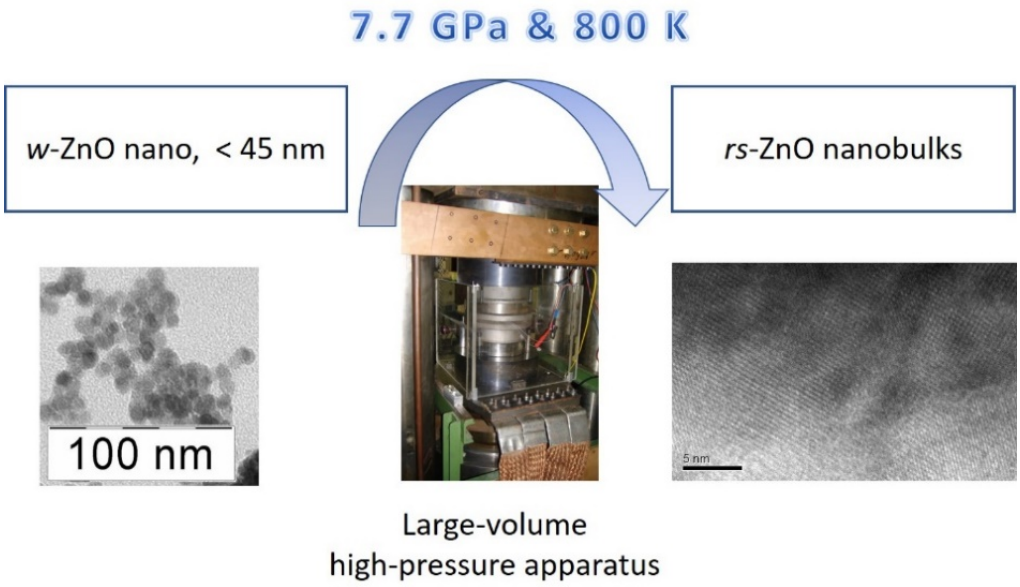

Figure 5. Synthesis scheme for single-phase rs-ZnO nanobulks.

Usually, as-synthesized rs-ZnO samples have a white nacreous color. In some cases (if initial nanocrystalline w-ZnO preliminary annealed in vacuum, etc.), yellowish translucent samples are obtained. The possibilities of the proposed method of synthesis of nanocrystalline rs-ZnO were tested for the production of single-phase rs-ZnO samples that were doped with 5-10 mol% MgO [40], 1% Fe_2O_3, 1% Eu_2O_3 and 1% Cr_2O_3. The color of the samples changed to snow-white, orange, purple and bright green, respectively. Thus, the proposed technique of the HP and HT synthesis of nanocrystalline cubic zinc oxide, allows the acquisition of doped rs-ZnO nanobulks as well.

The synthesis of rs-ZnO nanocrystalline bulks in large-volume high-pressure apparatuses [17] made it possible to experimentally study its properties at ambient pressure [75–77]. Low-temperature heat capacities (C_p) of rs-ZnO and w-ZnO nanobulks were measured in the 2–315 K temperature range [75]. No significant influence of nanostructuring on C_p of w-ZnO was observed. The measured C_p of rock-salt ZnO is lower than that of wurtzite ZnO below 100 K and higher above this temperature. The thermal expansion of rs-ZnO in the 10–300 K temperature range was also studied [76]. No phase transition was observed down to 10 K. The shape of the reduced thermal expansion curve of rs-ZnO is like those of other metal monoxides with a rock-salt structure, i.e., CaO, MgO and BaO [76]. The thermal stability of rs-ZnO nanobulks was studied by DSC [12,77] and powder X-ray diffraction [12]. It was shown that pure rs-ZnO is kinetically

stable up to ~370 K. When doped with magnesium, the thermal stability of rs-ZnO nanobulks increases up to 500 K [40].

According to our estimation, the standard enthalpy of the *w*-ZnO-to-*rs*-ZnO phase transition ($\Delta_{tr}H^0$(298.15 K) = 11.7 ± 0.3 kJ mol^{-1}) derived from experimental data [77] is two times lower than the "recommended" value ($\Delta_{tr}H^0$(298.15 K) = 23.93 ± 3.11 kJ mol^{-1}) suggested in [78] under the unfounded suggestion that P_{tr} = 9.6 GPa. Indeed, it is known that *w*-ZnO starts to transform to *rs*-ZnO that is already at pressures above 5 GPa [79]. At room temperature, this transition is very sluggish due to the existence of a strong kinetic barrier which hinders the nucleation of a new phase [79]. The obtained results have shown that below 1000 K the wurtzite-to-rock-salt phase transition in ZnO has pronounced diffusionless features. At the same time, due to the intensification of solid-state self-diffusion ZnO recrystallization has been observed already at 800 K [79]. Thus, the most reasonable choice for the transition pressure at 300 K is ~5.8 GPa.

Another important aspect concerning the thermodynamics of w-ZnO is the sign of the Clausius-Clapeyron slope (see Equation (1)). From the available literature data, one can confidently predict that the w-ZnO melting temperature will decrease under pressure (dT/dP < 0). The specific volume of the hypothetical liquid phase of ZnO (V_{liquid}) was estimated to be 13.5(5) or 13.8(5) cm^3/mole at 1500 K [80], whereas the specific volume of solid w-ZnO (V_{solid}) which can be estimated from the thermal expansion data [81] is 14.8(1) cm^3/mole at 1500 K. The zinc oxide melting enthalpy ($\Delta H_{melting}$) at pressures close to 0.1 MPa is 38 [82], 52.3 [83], 70 ± 10 [84] or 75.3 [85] kJ/mole which gives a variation of the dT/dP slope value from −32 to −100 K/GPa.

$$\frac{dT}{dP} = \frac{T_{melting}}{\Delta H_{melting}}(V_{liquid} - V_{solid}) \quad (1)$$

2.5. Melting and Crystallization of Zinc Oxide under Pressure—Growth of Single Crystals

Consider the possibility of using high pressure for the growth of ZnO single crystals. As is known from the literature, the triple point of zinc oxide is located at 2248(25) K and 1.06 bar [18]. To prevent the evaporation and dissociation of this compound at high temperatures it is necessary to maintain an oxygen overpressure. The approach suggested in [86] is essentially different from all previously used methods of zinc oxide single-crystal growth and implies crystallization from the melt at 4.2 GPa and ~1700 K. The method is based on the discovered decrease in ZnO melting point under pressure [86]. As was shown by synchrotron X-ray diffraction, at 4.2 GPa starting from 1600 K the temperature increase is accompanied by a decrease in the intensity of ZnO diffraction lines, and their complete disappearance is observed at 1713 K which is indicative of the melting. Thus, the melting temperature of ZnO was estimated as 1700 ± 10 K which is 550 K less than that at ambient pressure. The melting is of a congruent nature. These data made it possible to justify the use of high pressures to significantly reduce the melting temperature of zinc oxide and carry out the growth of ZnO single crystals by rapid spontaneous crystallization from the melt in a large-volume high-pressure apparatus [86].

The grown ZnO crystals were transparent, pale green or colorless, had a needle-like shape (2 mm in length and 0.2 mm in diameter) and well-defined coaxial growth orientation with respect to the compression axis (Figure 6). The wurtzite structure ($P6_3mc$) was confirmed by single-crystal X-ray diffraction which showed narrow line widths and an absence of twins. The cell parameters (a = 3.2474(5) Å, c = 5.2017(7) Å; V = 47.506(7) Å^3) are in good agreement with the literature values.

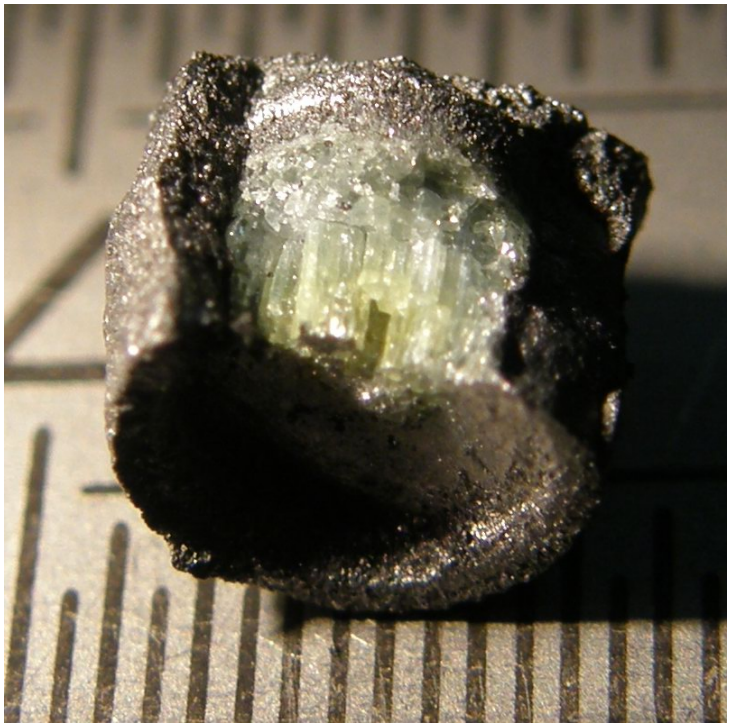

Figure 6. Microphotograph of zinc oxide single crystals grown from melt at high pressure (in the opened graphite heater after extraction from the high-pressure cell; scale value is 0.5 mm).

The photoluminescence (PL) spectra of the grown crystals consist of a strong violet emission peak at 398 nm and a relatively weak and broad green-yellow emission with maximum at ~600 nm which is typical for w-ZnO single crystals. The violet PL line corresponds to the near-band-edge emission in w-ZnO, indicating the formation of defect centers. An interesting feature was the observation of a linear dependence of PL intensity at 398 nm on the excitation power with a tendency towards saturation. This can be explained by the processes of the collective recombination of photoexcited charge carriers or stimulated light emission. This effect is consistent with the elongated and close-to-cylindrical shape of the studied single crystals. Thus, the w-ZnO single crystals grown at HP and HT have potential application for short-wavelength light emitting devices.

2.6. Growth of Doped ZnO Single Crystals under Pressure

Since the growth of single crystals occurs through the melt we can expect a homogeneous distribution of impurities when the melting temperatures of all introduced components are reached. Moreover, an important advantage of such a method of producing doped semiconductors as compared with solid-phase synthesis is the fact that during zinc oxide crystallization all excessive impurities will precipitate as an impurity phase without affecting the properties of grown single crystals. Moreover, the doping level will depend exclusively on the chemical nature of the introduced dopant. Another important advantage of this technique is that a high-pressure cell is closed in terms of exchange with the environment, i.e., there is no interaction with the atmosphere. In addition, there are no restrictions on any possible combination of several components if this is required. One example of such a growth of single crystals in the presence of other oxides was the growth of ZnO:Yb_2O_3 single crystals from the melt of a mixture of ZnO and Yb_2O_3 oxides (2%) at 3.8 GPa and 1700 K [87].

When ytterbium oxide is present in the initial mixture the growth of ZnO single crystals occurs by another mechanism. When ZnO melts under high pressure the ytterbium oxide dissolves in the zinc oxide melt. On cooling, the Yb_2O_3 crystallizes from this

melt and forms many nuclei on which ZnO single crystals start to grow. The dissolution of ytterbium oxide in the zinc oxide melt and its subsequent prior crystallization clearly follows from the analysis of SEM microphotographs. The fact that Yb_2O_3 particles are on the surface of zinc oxide single crystals was confirmed by elemental analysis carried out by energy-dispersive microanalysis in an electron microscope [88]. Thus, one can conclude that growth of zinc oxide single crystals from melts containing ytterbium oxide occurs under conditions of mass nucleation on Yb_2O_3 nanoparticles, leading to a significant decrease in the size of ZnO single crystals, compared to undoped zinc oxide. Similar results were observed in the presence of magnesium oxide and cadmium oxide.

The problem of producing stable and reproducible p-type ZnO crystals is still a challenge for experimenters. This difficulty is associated with the self-compensation, low solubility and high ionization energy of all possible acceptor dopants. Among the potential candidates of zinc oxide doping for p-type, the group V elements (P, As, Sb) attracted particular attention because of the predicted existence of the defect complex $Sb(P,As)_{Zn}$-$2V_{Zn}$ which is responsible for acceptor properties in ZnO. This was shown in several works on phosphorus, arsenic and antimony doping [88]. However, the majority of such doped ZnO materials were produced in the form of thin films, nanorods and nanobelts. Very recently, ZnO single crystals that were doped with group-V elements (P, As and Sb) have been grown from the melt at ~4 GPa [89]. Under UV excitation the grown crystals exhibit photoluminescence in the visible light (a yellow band with the maximum at 565 nm) which originates from V_{Zn}-associated acceptors. The number of V_{Zn} induced per one atom of dopant is significantly higher than 2 as in the $As(Sb)_{Zn}$-$2V_{Zn}$ complex. Other V_{Zn}-complexes such as $(V_{Zn}^{-})_2$ are generated as well which does not happen without doping. These results indicate that such doping indeed creates acceptor centers in ZnO single crystals.

3. Conclusions

The use of high pressures is an effective tool for solving several problems in the field of semiconductor material science—particularly, for producing new ZnO solid solutions, stabilizing metastable cubic zinc oxide and growing both doped and undoped ZnO single crystals. Solid solutions of zinc oxide with other metal oxides can be applied as ionic conductors, photocatalysts, thermoelectric materials and semiconductors with magnetic properties. Zinc oxide phase is a model object for studies of thermodynamics and the kinetics of phase transitions at high pressure that should result in the construction of an equilibrium P-T phase diagram of ZnO in a wide pressure- temperature range. Based on the study of thermodynamic properties, a decrease in the melting temperature of zinc oxide was discovered and the method of single crystals growth at high pressures was developed. This method is a unique way to produce single crystals because it allows the introduction of the desired impurity (or even several in any combination) which opens up the prospect of controlling the semiconductor (in particular, transport) properties of zinc oxide. This will enable the construction of devices based on p-n junction, such as LEDs and solar cells.

Author Contributions: Conceptualization, V.L.S. and A.N.B.; methodology, A.N.B. and V.L.S.; formal analysis, P.S.S. and A.N.B.; data curation, P.S.S. and A.N.B.; validation, A.N.B. and V.L.S.; resources, V.L.S. and A.N.B.; writing—original draft preparation, A.N.B. and P.S.S.; writing—review and editing, V.L.S.; visualization, P.S.S.; supervision, V.L.S. All authors have read and agreed to the published version of the manuscript.

Funding: This research received no external funding.

Conflicts of Interest: The authors declare no conflict of interest.

References

1. Pearton, S.J.; Jagadish, C. *Zinc Oxide: Bulk, Thin Films and Nanostructures*, Elsevier: Amsterdam, The Netherlands, 2006. https://doi.org/10.1016/B978-0-08-044722-3.X5000-3.
2. Ozgur, U.; Alivov, Y.I.; Liu, C.; Teke, A.; Reshchikov, M.A.; Dogan, S.; Avrutin, V.; Cho, S.-J.; Morkoc, H. A comprehensive review of ZnO materials and devices. *J. Appl. Phys.* **2005**, *98*, 041301. https://doi.org/10.1063/1.1992666.
3. Kołodziejczak-Radzimska, A.; Jesionowski, T. Zinc Oxide—From Synthesis to Application: A Review. *Materials* **2014**, *7*, 2833–2881. https://doi.org/10.3390/ma7042833.
4. Janotti, A.; Van de Walle, C.G. Fundamentals of zinc oxide as a semiconductor. *Rep. Prog. Phys.* **2009**, *72*, 126501. https://doi.org/10.1088/0034-4885/72/12/126501.
5. Liu, C.; Yun, F.; Morkoc, H. Ferromagnetism of ZnO and GaN: A Review. *J. Mater. Sci. Mater. Electron.* **2005**, *16*, 555–597. https://doi.org/10.1007/s10854-005-3232-1.
6. *Bates,* C.H.; White, W.B.; Roy, R. New high-pressure polymorph of zinc oxide. *Science* **1962**, *137*, 993. https://doi.org/10.1126/science.137.3534.993.a.
7. Bates, C.H.; White, W.B.; Roy, R. The solubility of transition metal oxides in zinc oxide and the reflectance spectra of Mn^{2+} and Fe^{2+} in tetrahedral fields. *J. Inorg. Nucl. Chem.* **1966**, *28*, 397–405. https://doi.org/10.1016/0022-1902(66)80318-4.
8. Ellmer, K.; Klein, A.; Rech, D. *Transparent Conductive Zinc Oxide*, Springer: Berlin, Germany, 2008 https://doi.org/10.1007/978-3-540-73612-7.
9. Kumar, N.; Yadav, S.; Mittal, A.; Kumari, K. Photocatalysis by zinc oxide-based nanomaterials. In *Nanostructured Zinc Oxide. Synthesis, Properties and Applications*; Awasthi, K., Ed.; Elsevier: Amsterdam, The Netherlands, 2021. https://doi.org/10.1016/B978-0-12-818900-9.00005-X.
10. Hoye, R.L.Z.; Musselman, K.P.; Macmanus-Driscoll, J.L. Research Update: Doping ZnO and TiO_2 for solar cells. *APL Mater.* **2013**, *1*, 060701. https://doi.org/10.1063/1.4833475.
11. Kunisu, M.; Tanaka, I.; Yamamoto, T.; Suga, T.; Mizoguchi, T. The formation of a rock-salt type ZnO thin film by low-level alloying with MgO. *J. Phys. Condens. Matter.* **2004**, *16*, 3801. https://doi.org/10.1088/0953-8984/16/21/028.
12. James Lu, C.-Y.; Tu, Y.-T.; Yan, T.; Trampert, A.; Chang, L.; Ploog, K.H. Growth and stability of rocksalt $Zn_{1-x}Mg_xO$ epilayers and ZnO/MgO superlattice on MgO (100) substrate by molecular beam epitaxy. *J. Chem. Phys.* **2016**, *144*, 214704. https://doi.org/10.1063/1.4950885.
13. Egbo, K.O.; Chibueze, T.C.; Raji, A.T.; Ekuma, C.E.; Liu, C.P.; Yu, K.M. Effects of acceptor doping and oxygen stoichiometry on the properties of sputter-deposited p-type rocksalt $Ni_xZn_{1-x}O$ ($0.3 \leq x \leq 1.0$) alloys. *J. Alloys Compd.* **2022**, *905*, 164224. https://doi.org/10.1016/j.jallcom.2022.164224.
14. Liu, C.P.; Egbo, K.O.; Ho, C.Y.; Wang, Y.; Xu, C.K.; Yu, K.M. Wide-Gap $Zn_{1-x}Ni_xO$ alloy: A transparent p-type oxide. *Phys. Rev. Appl.* **2020**, *13*, 024049. https://doi.org/10.1103/PhysRevApplied.13.024049.
15. Baranov, A.N.; Solozhenko, V.L.; Chateau, C.; Bocquillon, G.; Petitet, J.P.; Panin, G.N.; Kang, T.W.; Shpanchenko, R.V.; Antipov, E.V.; Oh, Y.J. Cubic $Mg_xZn_{1-x}O$ wide band gap solid solutions synthesized at high pressures. *J. Phys. Cond. Matter.* **2005**, *7*, 3377–3384. https://doi.org/10.1088/0953-8984/17/21/030.
16. Solozhenko, V.L.; Baranov, A.N.; Turkevich, V.Z. High-pressure formation of $Mg_xZn_{1-x}O$ solid solutions with rock salt structure. *Solid State Comm.* **2006**, *138*, 534–537. https://doi.org/10.1016/j.ssc.2006.04.005.
17. Baranov, A.N.; Sokolov, P.S.; Tafeenko, V.A.; Lathe, C.; Zubavichus, Y.V.; Veligzhanin, A.A.; Chukichev, M.V.; Solozhenko, V.L. Nanocrystallinity as a route to metastable phases: Rock salt ZnO. *Chem. Mat.* **2010,** *25*, 1775–1782. https://doi.org/10.1021/cm400293j.
18. Klimm, D.; Ganschow, S.; Schulz, D.; Fornari, R. The growth of ZnO crystals from the melt. *J. Cryst. Growth* **2008**, *310*, 3009–3013. https://doi.org/10.1016/j.jcrysgro.2008.02.027.
19. Kusaba, K.; Syonom, Y.; Kikegawam, T. Phase transition of ZnO under high pressure and temperature. *Proc. Jpn. Acad. Ser. B* **1999**, *75*, 1–6. https://doi.org/10.2183/pjab.75.1.
20. Norton, D.P.; Heo, Y.W.; Ivill, M.P.; Ip, K.; Pearton, S.J.; Chisholm, M.F.; Steiner, T. ZnO: Growth, doping and processing. *Mater. Today* **2004**, *7*, 34–40. https://doi.org/10.1016/S1369-7021(04)00287-1.
21. Norton, D.P.; Pearton, S.J.; Hebard, A.F.; Theodoropoulou, N.; Boatner, L.A.; Wilson, R.G. Ferromagnetism in Mn-implanted ZnO:Sn single crystal. *Appl. Phys. Lett.* **2003**, *82*, 239–241. https://doi.org/10.1063/1.1537457.
22. Fukumura, T.; Toyosaki, H.; Yamada, Y. Magnetic oxide semiconductors. *Semicond. Sci. Technol.* **2005**, *20*, S103–S111. https://doi.org/10.1088/0268-1242/20/4/012.
23. Makino, T.; Segawa, Y.; Kawasaki, M.; Ohtomo, A.; Shiroki, R.; Tamura, K.; Yasuda, T.; Koinuma, H. Band gap engineering based on $Mg_xZn_{1-x}O$ and $Cd_yZn_{1-y}O$ ternary alloy films. *Appl. Phys. Lett.* **2001**, *78*, 1237–1239. https://doi.org/10.1063/1.1350632.
24. Decremps, F.; Zhang, J.; Liebermann, R.C. New phase boundary and high-pressure thermoelasticity of ZnO. *Europhys. Lett.* **2000**, *51*, 268–274. https://doi.org/10.1209/epl/i2000-00347-0.
25. Davies, P.K.; Navrotsky, A. Thermodynamics of solid solution formation in NiO-MgO and NiO-ZnO. *J. Solid State Chem.* **1981**, *38*, 264–276. https://doi.org/10.1016/0022-4596(81)90044-X.
26. Seko, A.; Obam, F.; Kuwabara, A.; Tanaka, I. Pressure-induced phase transition in ZnO and ZnO-MgO pseudobinary system: A first-principles lattice dynamics study. *Phys. Rev. B* **2005**, *72*, 024107. https://doi.org/10.1103/PhysRevB.72.024107.

27. Sowa, H.; Ahsbahs, H. High-pressure X-ray investigation of zincite ZnO single crystal using diamond anvils with an improved shape. *J. Appl. Crystallogr.* **2006**, *39*, 169–175. https://doi.org/10.1107/S0021889805042457.
28. Decremps, F.; Zhang, J.; Li, B.; Liebermann, R.C. Pressure-induced softening of shear modes in ZnO. *Phys. Rev. B* **2002**, *63*, 224105. https://doi.org/10.1103/PhysRevB.66.174106.
29. Segura, A.; Sans, J.A.; Manjon, F.J.; Munoz, A.; Herrera-Cabrera, M.J. Optical properties and electronic structure of rock-salt ZnO under pressure. *Appl. Phys. Lett.* **2003**, *83*, 278–280. https://doi.org/10.1063/1.1591995.
30. Sans, J.A.; Segura, A.; Manjon, F.J.; Mari, B.; Munoz, A.; Herrera-Cabrera, M.J. Optical properties of wurtzite and rock-salt ZnO under pressure. *Microelectr. J.* **2005**, *36*, 928–932. http://doi.org/10.1016/j.mejo.2005.05.010.
31. Jiang, J.Z.; Olsen, J.S.; Gerward, L.; Frost, D.; Rubie, D.; Peyronneau, J. Structural stability in nanocrystalline ZnO. *Europhys. Lett.* **2000**, *50*, 48–53. https://doi.org/10.1209/epl/i2000-00233-9.
32. Yu, C.; Yu, Q.; Gao, C.; Yang, H.; Li, B.; Peng, G.; Han, Y.; Zhang, D.; Cui, X.; Liu, C.; Wang, Y. Phase transformation and resistivity of dumbbell-like ZnO microcrystals under high pressure. *J. Appl. Phys.* **2008**, *103*, 114901. https://doi.org/10.1063/1.2931039.
33. Decremps, F.; Datchi, F.; Saitta, A.M.; Polian, A.; Pascarelli, S.; Di Cicco, A.; Itie, J.P.; Baudelet, F. Local structure of condensed zinc oxide. *Phys. Rev. B.* **2003**, *68*, 104101. https://doi.org/10.1103/PhysRevB.68.104101.
34. Karzel, H.; Potzel, W.; Köfferlein, M.; Schiessl, W.; Steiner, M.; Hiller, U.; Kalvius, G.M.; Mitchell, D.W.; Das, T.P., Blaha, P.; et al. Lattice dynamics and hyperfine interactions in ZnO and ZnSe at high external pressures. *Phys. Rev. B* **1996**, *53*, 11425–11438. https://doi.org/10.1103/PhysRevB.53.11425.
35. Decremps, F.; Pellicer-Porres, J.; Marco Saitta, A.; Chervin, J.-C.; Polian, A. High-pressure Raman spectroscopy study of wurtzite ZnO. *Phys. Rev. B.* **2002**, *65*, 092101. https://doi.org/10.1103/PhysRevB.65.092101.
36. Manjon, F.J.; Syassen, K.; Lauck, R. Effect of pressure on phonon modes in wurtzite zinc oxide. *High Pressure Res*. **2002**, *22*, 299–304. http://doi.org/10.1080/08957950212798.
37. Bayarjargal, L.; Winkler, B.; Haussuhl, E.; Boehler, R. Influence of deviatoric stress on the pressure-induced structural phase transition of ZnO studied by optical second harmonic generation measurements. *Appl. Phys. Lett.* **2009**, *95*, 061907. https://doi.org/10.1063/1.3205120.
38. Jiang, J.Z.; Gerward, L.; Frost, D.; Secco, R.; Peyronneau, J.; Olsen, J.S. Grain-size effect on pressure-induced semiconductor-to-metal transition in ZnS. *J. Appl. Phys.* **1999**, *86*, 6608–6610. https://doi.org/10.1063/1.371631.
39. Baranov, A.N.; Sokolov, P.S.; Kurakevych, O.O.; Tafeenko, V.A.; Trots, D.; Solozhenko, V.L. Synthesis of rock-salt MeO–ZnO solid solutions (Me= Ni^{2+}, Co^{2+}, Fe^{2+}, Mn^{2+}) at high pressure and high temperature. *High Pressure Res.* **2008**, *4*, 515. https://doi.org/10.1080/08957950802379307.
40. Sokolov, P.S. The synthesis of cubic ZnO and its solid solutions at high pressures and high temperatures. Ph.D. Thesis, Université Paris Nord, Villetaneuse, France, 2010.
41. Bhadram, V.S.; Cheng, Q.; Chan, C.K.; Liu, Y.; Lany, S.; Landskron, K.; Strobel, T.A. $Zn_xMn_{1-x}O$ solid solutions in the rocksalt structure: Optical, charge transport, and photoelectrochemical properties *ACS Appl. Energy Mater.* **2018**, *1*, 260. https://doi.org/10.1021/acsaem.7b00084.
42. Sokolov, P.S.; Baranov, A.N.; Lathe, C.; Solozhenko, V.L. High-pressure synthesis of FeO–ZnO solid solutions with rock salt structure: In situ X-ray diffraction studies. *High Press. Res.* **2010**, *30*, 39–43. https://doi.org/10.1080/08957950903550236.
43. Sokolov, P.S.; Baranov, A.N.; Lathe, C.; Turkevich, V.Z.; Solozhenko, V.L. High-pressure synthesis of MnO–ZnO solid solutions with rock salt structure: In situ X-ray diffraction studies. *High Press. Res.* **2011**, *31*, 43–47. https://doi.org/10.1080/08957959.2010.521653.
44. Sokolov, P.S.; Baranov, A.N.; Tafeenko, V.A.; Solozhenko, V.L. High pressure synthesis of $LiMeO_2$–ZnO (Me=Fe^{3+}, Ti^{3+}) solid solutions with a rock salt structure. *High Press. Res.* **2011**, *31*, 304–309. https://doi.org/10.1080/08957959.2011.560844.
45. Shannon, R.D. Revised effective ionic radii and systematic studies of interatomic distances in halides and chalcogenides. *Acta Crystallogr. A* **1976**, *32*, 751–767. https://doi.org/10.1107/S0567739476001551.
46. Raghavan, S.; Hajra, J.P.; Iyengar, G.N.K.; Abraham, K.P. Terminal solid solubilities at 900–1000 °C in the magnesium oxide-zinc oxide system measured using a magnesium fluoride solid-electrolyte galvanic cell. Thermochim. Acta **1991**, 189, 151–158. https://doi.org/10.1016/0040-6031(91)87109-A.
47. Sokolov, P.S.; Baranov, A.N.; Dobrokhotova, Z.V.; Solozhenko, V.L. Synthesis and thermal stability of cubic ZnO in the salt nanocomposites. *Russ. Chem. Bull.* **2010**, *59*, 325–328. https://doi.org/10.1007/s11172-010-0082-7.
48. Sokolov, P.S.; Baranov, A.N.; Tafeenko, V.A.; Solozhenko, V.L. Synthèse des solutions solides cubiques ZnO-$LiMeO_2$ (Me = Sc^{3+}, Ti^{3+}, Fe^{3+}, In^{3+}) sous hautes pressions et hautes températures. In Proceedings of the 7e Forum de Technologie des Hautes Pressions, Biarritz, France, 11–15 Octobre 2010.
49. Fernandes, A.A.R.; Santamaria, J.; Bud'ko, S.L.; Nakamura, O.; Guimpel, J.; Schuller, I.K. Effect of physical and chemical pressure on the superconductivity of high-temperature oxide superconductors. *Phys. Rev. B.* **1991**, *44*, 7601. https://doi.org/10.1103/PhysRevB.44.7601.
50. Urusov, V.S. Interaction of Cations on Octahedral and Tetrahedral Sites in Simple Spinels. Phys. Chem. Miner. **1983**, 10, 194–195. https://doi.org/10.1007/BF00309461.
51. Maksimov, V.I.; Dubinin, S.F.; Baranov, A.N.; Sokolov, V.I.; Sokolov, P.S.; Parkhomenko, V.D. Structural state of metastable cubic compounds $Ni_{1-x}Zn_xO$ ($0.6 \le x \le 0.99$). *Phys. Met. Metallogr.* **2013**, *114*, 734–740. https://doi.org/10.1134/S0031918X13060094.

52. Dubinin, S.F.; Maksimov, V.I.; Parkhomenko, V.D.; Sokolov, V.I.; Baranov, A.N.; Sokolov, P.S.; Dorofeev, Y.A. Fine structure and magnetism of the cubic oxide compound $Ni_{0.3}Zn_{0.7}O$. *Phys. Solid State* **2011**, *53*, 1362–1366. https://doi.org/10.1134/S1063783411070092.
53. Gurskiy, S.I.; Tafeenko, V.A.; Baranov, A.N. Use of integrated intensities of X-ray powder diffraction patterns of $Mg_{1-x}Zn_xO$ solid solutions for the quantitative determination of their composition. *Russ. J. Inorg. Chem.* **2008**, *53*, 111–116. https://doi.org/10.1134/S0036023608010154.
54. Babanov, Y.A.; Ponomarev, D.A.; Ustinov, V.V. Visualization of the atomic structure of solid solutions with the NaCl structure. *Phys. Solid State.* **2015**, 57, 717–721. https://doi.org/10.1134/S106378341504006X.
55. Babanov, Y.A.; Ponomarev, D.A.; Ustinov, V.V.; Baranov, A.N.; Zubavichus, Y.V. Local atomic structure of solid solutions with overlapping shells by EXAFS: The regularization method. *J. Electron Spectrosc.* **2016**, *211*, 1–11. https://doi.org/10.1016/j.elspec.2016.03.003.
56. Sokolov, V.I.; Pustovarov, V.A.; Churmanov, V.N.; Ivanov, V.Y.; Gruzdev, N.B.; Sokolov, P.S.; Baranov, A.N.; Moskvin, A.S. Unusual x-ray excited luminescence spectra of NiO suggest self-trapping of the d-d charge-transfer exciton. *Phys. Rev. B.* **2012**, *86*, 115128. https://doi.org/10.1103/PhysRevB.86.115128.
57. Sokolov, V.I.; Pustovarov, V.A.; Churmanov, V.N.; Ivanov, V.Y.; Gruzdev, N.B.; Sokolov, P.S.; Baranov, A.N.; Moskvin, A.S. Self-trapping of the d-d charge transfer exciton in bulk NiO evidenced by X-ray excited luminescence. *Jetp Lett.* **2012**, *95*, 528–533. https://doi.org/10.1134/S0021364012100116.
58. Sokolov, V.I.; Pustovarov, V.A.; Churmanov, V.N.; Ivanov, V.Y.; Gruzdev, N.B.; Sokolov, P.S.; Baranov, A.N.; Moskvin, A.S. Self-trapping of the d-d charge transfer exciton in rock-salt structured $Zn_{1-x}Ni_xO$ evidenced by soft X-ray excited luminescence *Phys. Status Solidi C.* **2013**, *10*, 1329–1335. https://doi.org/10.1002/pssc.201200980.
59. Sokolov, V.I.; Pustovarov, V.A.; Ivanov, V.Y.; Gruzdev, N.B.; Sokolov, P.S.; Baranov. A.N. The influence of temperature on narrow I_1 and I_2 lines in the luminescence spectrum of $Ni_{0.6}Zn_{0.4}O$. *Opt. Spectrosc.* **2014**, *116*, 798–801. https://doi.org/10.1134/S0030400X14050245.
60. Churmanov, V.N.; Sokolov, V.I.; Gruzdev, N.B.; Ivanov, V.Y.; Pustovarov, V.A. Exciton lines in luminescence spectra of NixZn1-xO under inner shell excitation. *Physcs. Proc.* **2015**, *76*, 120–124. https://doi.org/10.1016/j.phpro.2015.10.022.
61. Sokolov, V.I.; Pustovarov, V.A.; Churmanov, V.N.; Gruzdev, N.B.; Uimin, M.A.; Byzov, I.V.; Druzhinin, A.V.; Mironova-Ulmane, N.A. Luminescence and optical spectroscopy of charge transfer processes in solid solutions $Ni_cMg_{1-c}O$ and $Ni_xZn_{1-x}O$. *J. Lumin.* **2016**, *169*, 641–644. https://doi.org/10.1016/j.jlumin.2015.03.039.
62. Churmanov, V.N.; Sokolov, V.I.; Gruzdev, N.B.; Ivanov, V.Y.; Pustovarov, V.A. p-d charge transfer excitons in $Zn_{1-x}Ni_xO$ under inner shell excitation. *Phys. Status Solidi C.* **2016**, *13*, 610–613. https://doi.org/10.1002/pssc.201510245.
63. Sarkar, A.; Wang, Q.; Schiele, A.; Chellani, M.R.; Bhattacharya, S.S.; Wang, D.; Brezesinski, T.; Hahn, H.; Velasco, L.; Breitung, B. High-entropy oxides: Fundamental aspects and electrochemical properties. *Adv. Mater.* **2019**, *31*, 1806236. https://doi.org/10.1002/adma.201806236.
64. Li, B.; Sougrati, M.T.; Rousse, G.; Morozov, A.V.; Dedryvere, R.; Iadecola, A.; Senyshyn, A.; Zhang, L.; Abakumov, A.A.; Doublet, M. et al. Correlating ligand-to-metal charge transfer with voltage hysteresis in a Li-rich rock-salt compound exhibiting anionic redox. *Nat. Chem.* **2021**, *13*, 1070–1080. https://doi.org/10.1038/s41557-021-00775-2.
65. Cambaz, M.A.; Vinayan, B.P.; Euchner, H.; Guda, A.A.; Mazilkin, A.; Rusalev, Y.V.; Trigub, A.L.; Gross, A.; Fichtner, M. Design of nickel-based cation-disordered rock-salt oxides: The effect of transition metal (M = V, Ti, Zr) substitution in $LiNi_{0.5}M_{0.5}O_2$ binary systems. *ACS Appl. Mater. Interfaces* **2018**, *10*, 21957–21964. https://pubs.acs.org/doi/abs/10.1021/acsami.8b02266.
66. Zhang, P.; Wang, Y.; Hua, Y.; Han, Y.; Li, L. Low-temperature sintering and microwave dielectric properties of $Li_2ZnTi_3O_8$ ceramics. *Mater. Lett.* **2013**, *107*, 351–353. https://doi.org/10.1016/j.matlet.2013.06.041.
67. Yuan, L.L.; Bian, J.J. Microwave dielectric properties of the lithium containing compounds with rock salt structure, Ferroelectrics **2009,** 387, 123–129. https://doi.org/10.1080/00150190902966610.
68. Viegas, J.I.; Moreira, R.L.; Dias, A. Optical-vibration properties of Li_2ZnGeO_4 dielectric ceramics. *Vib. Spectrosc.* **2020**, *110*, 103130. https://doi.org/10.1016/j.vibspec.2020.103130.
69. Zhao, Y.; Zhang, P. Microstructure and microwave dielectric properties of low loss materials $Li_3(Mg_{0.95}A_{0.05})_2NbO_6$ (A = Ca^{2+}, Ni^{2+}, Zn^{2+}, Mn^{2+}) with rock-salt structure. *J. Alloys Compds.* **2016**, *658*, 744–748. https://doi.org/10.1016/j.jallcom.2015.10.249.
70. Kumar, R.S.; Cornelius, A.L.; Nicol, A.F. Structure of nanocrystalline ZnO up to 85 GPa. *Curr. Appl. Phys.* **2007**, *7*, 135–138. https://doi.org/10.1016/j.cap.2006.02.009.
71. Grzanka, E.; Gierlotkam, S.; Stelmakh, S.; Palosz, B.; Strachowski, T.; Swiderska-Srode, A.; Kalisz, G.; Lojkowski, W.; Porsch, F. Phase transition in nanocrystalline ZnO. *Z. Kristallogr.* **2006**, *23*, 337–342. https://doi.org/10.1524/9783486992526-057.
72. Bayarjargal, L.; Wiehl, L.; Winkler, B. Influence of grain size, surface energy, and deviatoric stress on the pressure-induced phase transition of ZnO and AlN. *High Press. Res.* **2013**, *33*, 642–651. https://doi.org/10.1080/08957959.2013.800514.
73. Gerward, L.; Olsen, J.S. The high-pressure phase of zincite. *J. Synchrotron Rad.* **1995**, *2*, 233–235. https://doi.org/10.1107/S0909049595009447.
74. Baranov, A.N.; Kurakevych, O.O.; Tafeenko, V.A.; Sokolov, P.S.; Panin, G.N.; Solozhenko, V.L. High-pressure synthesis and luminescent properties of cubic ZnO/MgO nanocomposites. *J. Appl. Phys.* **2010**, *107*, 073519. https://doi.org/10.1063/1.3359661.
75. Kamenev, K.V.; Courac, A.; Sokolov, P.S.; Baranov, A.N.; Sharikov, F.Y.; Solozhenko, V.L. Heat capacities of nanostructured wurtzite and rock salt ZnO: Challenges of ZnO nano-phase diagram. *Solids* **2021**, *2*, 121–128. https://doi.org/10.3390/solids2010007.

76. Sokolov, P.S.; Baranov, A.N.; Bell, A.M.T.; Solozhenko, V.L. Low-temperature thermal expansion of rock-salt ZnO. *Solid State Commun.* **2014**, *177*, 65–67. https://doi.org/10.1016/j.ssc.2013.10.006.
77. Sharikov, F.Y.; Sokolov, P.S.; Baranov, A.N.; Solozhenko, V.L. On the thermodynamic aspect of zinc oxide polymorphism: Calorimetric study of metastable rock salt ZnO. *Mendeleev Commun.* **2017**, *27*, 613–614. https://doi.org/10.1016/j.mencom.2017.11.025.
78. Leitner, J.; Kamrádek, M.; Sedmidubský, D. Thermodynamic properties of rock-salt ZnO. *Thermochim. Acta* **2013**, *572*, 1–5. https://doi.org/10.1016/j.tca.2013.08.004.
79. Solozhenko, V.L.; Kurakevych, O.O.; Sokolov, P.S.; Baranov, A.N. Kinetics of the wurtzite to rock-salt phase transformation in ZnO at high pressure. *J. Phys. Chem. A* **2011**, *115*, 4354–4358. https://doi.org/10.1021/jp201544f.
80. Potuzak, M.; Dingwell, D.B.; Ledda, B.; Courtial, P. A partial molar volume for ZnO in silicate melts. *Am. Mineral*. **2006**, *91*, 366. https://doi.org/10.2138/am.2006.1817.
81. Iwanaga, H.; Kunishige, A.; Takeuchi, S. Anisotropic thermal expansion in wurtzite-type crystals. *J. Mater. Sci*. **2000**, *35*, 2451. https://doi.org/10.1023/A:1004709500331.
82. Belov, G.V.; Iorish, V.S.; V.S. Yungman, IVTANTHERMO for Windows—Database on thermodynamic properties and related software. *Calphad* **1999**, *23*, 173. Thermodynamic data for w-ZnO and Liquid-ZnO. Available online: http://www.chem.msu.su/rus/handbook/ivtan/263.html (accessed on 20 May 2022).
83. Batsanov, S.S. *Structural Chemistry. Book of Facts.*; Dialog-MSU: Moscow, Russia, 2000; p. 37, table 1.27 (Data of National Metrological Institute of Russia, VNIIFRTI). Available online: http://www.chem.msu.su/rus/elibrary/bazanov/welcome.html (accessed on 20 May 2022).
84. Thermodynamic Properties of Individual Substances (TSIV) Database (in Russian). Available online: http://www.chem.msu.su/rus/tsiv/Zn/ZnO_c.html (accessed on 20 May 2022).
85. Kerridge, D.H.; Sturton, I.A. Fused zinc chloride part II: Some solubility measurements. *Inorg. Chim. Acta* **1974**, *8*, 27–30. https://doi.org/10.1016/S0020-1693(00)92591-X.
86. Mukhanov, V.A.; Sokolov, P.S.; Baranov, A.N.; Timoshenko, V.Y; Zhigunov, D.M.; Solozhenko, V.L. Congruent melting and rapid single-crystal growth of ZnO at 4 GPa. *CrystEngComm* **2013**, *32*, 6318–6322. https://doi.org/10.1039/C3CE40766G.
87. Baranov, A.N.; Shestakov, M.V.; Chukichev, M.V.; Tafeenko, V.A.; Mukhanov, V.A.; Solozhenko, V.L. Cathodoluminescence of zinc and ytterbium oxide poly- and single crystals grown from melt under high pressure. *Trends Phys. Chem.* **2021**, 21, 81–86.
88. Fan, J.C.; Sreekanth, K.M.; Xie, Z.; Chang, S.L.; Rao, K.V. p-Type ZnO materials: Theory, growth, properties and devices. *Prog. Mater. Sci.* **2013**, *58*, 874–985. http://doi.org/10.1016/j.pmatsci.2013.03.002.
89. Taibarei, N.O.; Kytin, V.G.; Konstantinova, E.A.; Kulbachinskii, V.A.; Shalygina, O.A.; Pavlikov, A.V.; Savilov, S.V.; Tafeenko, V.A.; Mukhanov, V.A.; Solozhenko, V.L.; et al. Doping nature of group V elements in ZnO single crystals grown from melts at high pressure. *Cryst. Growth Des.* **2022**, *22*, 2452–2461. https://doi.org/10.1021/acs.cgd.1c01507.